Editors' Suggestion

Heat transfer from an array of resolved particles in turbulent flow

Yayun Wang*
Department of Mechanical Engineering, Johns Hopkins University, 3400 North Charles Street, Baltimore, Maryland 21218, USA

Andrea Prosperetti†
Department of Mechanical Engineering, University of Houston, 4726 Calhoun Rd, Houston, Texas 77204-4006, USA
and Faculty of Science and Technology and J. M. Burgers Centre for Fluid Dynamics, University of Twente, P.O. Box 217, 7500 AE Enschede, the Netherlands

(Received 18 February 2018; published 29 August 2018)

The PHYSALIS method for resolved numerical simulation of particulate flows, recently extended to include particles-fluid heat transfer, is applied to the turbulent flow past a planar particle array perpendicular to the incoming mean flow. The array consists of nine equal spheres. Periodicity boundary conditions are imposed on the boundaries of the computational domain parallel to the mean flow. The Reynolds number based on the particle diameter and mean incident flow is 120, the Taylor-scale Reynolds number is close to 30, and the ratio of particle radius to the Kolmogorov length is about 10. A detailed characterization of the flow and heat transfer is given including probability distribution functions of temperature and streamwise velocity, contour maps of the temperature fluctuations, diagonal Reynolds stresses, turbulent heat flux, and the various contributions to the energy budget. Turbulence moderately increases the heat transfer and considerably shortens the thermal wake of the particles. Temperature and streamwise velocity develop very differently downstream of the spheres in spite of the fact that the Prandtl number equals 1, because of the blockage by the spheres, which has no counterpart for the temperature.

DOI: 10.1103/PhysRevFluids.3.084305

I. INTRODUCTION

Much of what is currently theoretically known about the thermo-fluid mechanics of the interaction of particles and a fluid is based on the point-particle model [1–3] or the discrete-element model [4,5]. Both approaches suffer from the use of parametrized expressions for the hydrodynamic force and heat transfer coefficient in place of their evaluation on the basis of first principles. A few resolved simulations of the flow past individual particles exist, in both the laminar [6–9] and turbulent [10–12] regimes, but these studies do not provide information on the effects of particle-particle interactions.

It is only recently that our understanding of these phenomena has begun to improve because of the development of various numerical methods capable of providing resolved simulations of flows with many particles [13–19], which have begun to be extended to simulate thermal, in addition to mechanical, interactions [20–31].

These studies have begun to open up this field, which is of obvious importance for many applications such as fluidized beds, cooling towers, cloud formation, and many others. Much work

*wangyayun1990@gmail.com; www.physaliscfd.org
†aprosper@central.uh.edu

still remains to be done. For example, while Ref. [11] studied a single particle in a turbulent flow, and others studied particle interactions in pseudoturbulence [27,29,31] and in fluidized-bedlike systems [28], no studies exist of particle interactions in a truly turbulent flow. The present study is a first contribution in this direction. By means of the recent extension of the PHYSALIS method to heat transfer problems [30], we carry out resolved simulations of a planar array of fixed particles immersed in a decaying turbulent flow. Our focus is providing detailed information on the flow and heat transfer processes rather than developing correlations for engineering use. A simple analytic point-particle model based on the Oseen equations sheds light on some of the results.

II. MATHEMATICAL MODEL AND NUMERICAL METHOD

We consider spherical particles in a nonisothermal, incompressible, constant properties Newtonian fluid. The Navier-Stokes equations are

$$\nabla \cdot \mathbf{u} = 0, \tag{1}$$

$$\frac{\partial \mathbf{u}}{\partial t} + \mathbf{u} \cdot \nabla \mathbf{u} = -\frac{1}{\rho} \nabla p + \nu \nabla^2 \mathbf{u}. \tag{2}$$

Here $\mathbf{u}$ and p are the velocity and pressue fields; the fluid density is denoted by ρ and the kinematic viscosity by ν. The energy equation is

$$\frac{\partial T}{\partial t} + \mathbf{u} \cdot \nabla T = D \nabla^2 T, \tag{3}$$

with T the temperature and $D = k/(\rho c_p)$ the thermal diffusivity of the fluid expressed in terms of the thermal conductivity k and specific heat c_p; viscous heating is neglected on account of the smallness of this effect.

For simplicity, the particle temperature will be taken as T_p, fixed and the same for all the particles. The heat flow rate *into* the particles Q is given by

$$Q = k \oint_{s_p} \nabla T \cdot \mathbf{n}_p \, ds_p, \tag{4}$$

where $s_p = 4\pi a^2$, with a the particle radius, is the particle surface and $\mathbf{n}_p$ is the outwardly directed unit normal. The instantaneous Nusselt number for each particle is defined by

$$\mathrm{Nu} = \frac{2aQ/s_p}{k(T_i - T_p)} = \frac{1}{2\pi a (T_i - T_p)} \oint_{s_p} \nabla T \cdot \mathbf{n}_p \, ds_p, \tag{5}$$

in which T_i is the temperature of the fluid far upstream of the particles.

The problem is solved numerically by the PHYSALIS method, which is described in detail in several papers [18,32] for what concerns the particles-fluid momentum interaction and, more recently, in Ref. [30] for what concerns the particles-fluid thermal interaction. The reader is referred to these papers for details. The general idea is to use analytic solutions for the velocity and temperature fields in the immediate neighborhood of each particle as "bridges" between the particle surface and the underlying fixed Cartesian grid. These analytic solutions, which exist locally near each particle because of the no-slip condition, are expressed in terms of series with unknown coefficients which are determined iteratively by matching the local solution to a discretized finite-difference solution of (1) to (3). The coefficients of the expansions embody directly, with no need for further calculations, important information on the particles-fluid interaction such as drag and lift forces and couple and heat transfer rate (as well as higher-order information such as stresslet and couplet). The no-slip condition is satisfied to analytic accuracy on the exact spherical surface of the particles whatever the order of truncation of the series. Another useful feature of the method is the exponential decrease of the error as the number of terms retained in the series is increased, which is quite unlike the algebraic

TABLE I. Characteristics of the incident turbulence at the particles plane; Re_λ is the Taylor Reynolds number, η is the Kolmogorov length, a the particle radius, τ_E the eddy turnover time, ℓ the integral length scale, and u' the root-mean-square turbulent velocity fluctuation.

Re_λ	a/η	$\tau_E \nu/a^2$	λ_g/a	ℓ/a	u'/U
30.2	10.4	0.114	1.07	2.18	45%

error decrease of other methods. This feature permits us to achieve excellent accuracy with relatively coarse discretizations.

III. DESCRIPTION OF THE SIMULATIONS

We simulate the decaying turbulent flow past an array of nine equal spherical particles arranged in a regular square array of side $d = 5a$ with centers on the plane $z = 0$ perpendicular to the mean velocity U of the incident flow. The particle Reynolds number based on the mean streamwise velocity U is $\mathrm{Re}_p = 2aU/\nu = 120$, and the turbulence Taylor Reynolds number at the particle plane is $\mathrm{Re}_\lambda = 30.2$. The Kolmogorov length scale is $\eta \simeq a/10$, and the Prandtl number $\mathrm{Pr} = 1$.

The computational domain is a parallelepiped with a square cross section with sides of length $15a$ in the cross-stream direction and a length of $24a$ in the flow direction. The particle array is centered on the parallelepiped cross section, with the outermost particles at a distance $d/2$ from the surfaces of the computational domain parallel to the flow. Thus, as far as the geometry is concerned, the situation considered is equivalent to the infinite repetition of a fundamental unit consisting of a parallelepiped with a square cross section of size $d \times d$ perpendicular to the mean flow and having a single particle on its axis. Since the flow is unsteady and turbulent, this periodicity holds only in a time-average sense but not instantaneously. On the sides of the computational domain parallel to the mean flow we impose periodicity conditions, which enforce instantaneous periodicity across these surfaces. At the exit of the computational domain the normal derivative of the normal velocity vanishes, and the in-plane derivatives of the tangential velocity components also vanish.

Isotropic, homogeneous turbulence with $\mathrm{Re}_\lambda = 43$ is generated in an auxiliary cubic domain with sides of length $15a$ using the linear forcing scheme of Ref. [33] (see also Refs. [34,35]). This turbulent field, augmented by a constant velocity U along the z direction, is then imposed at the inlet of the primary domain containing the particles, in the manner described in Ref. [36] and Ref. [37]. The eddy turnover time is 3.5 times shorter than the convection time over the length of the computational domain, which ensures the absence of artificial periodicity as discussed in Ref. [36]. We checked that the features of the turbulence, and in particular the intensity and integral length scale, matched the results reported in Ref. [34]. The characteristics of the incident flow at the plane occupied by the particles are summarized in Table I.

The particle centers are at a distance of $4.5a$ from the inlet face of the domain, which is sufficient to avoid interference between the particles and the inlet boundary condition. The incident flow is at the reference temperature T_i while all the particles are kept at a fixed temperature $T_p < T_i$. In order to calculate reasonably converged average values, we performed simulations corresponding to 10 different realizations of the incident turbulent flow, each one lasting 45 eddy turnover times τ_E. Averages were collected excluding an initial period of duration $10\tau_E$. For each realization, we performed two different simulations, with and without the particles in place. The latter simulations were used to characterize the flow incident on the particles. Another simulation of the laminar flow at the same particle Reynolds number was also run.

In the numerical implementation of the PHYSALIS method we used 15 cells per radius to guarantee an adequate description of the interaction of the particles with the intense turbulent gusts by which it is buffeted. The Lamb series on which the method is based (see also Ref. [18]) was truncated at level

2 for the momentum and 4 for the temperature. The total number of cells was $180 \times 180 \times 288$, and the Courant number was 0.5.

In view of the periodicity conditions on the lateral surfaces, upon integrating the momentum equation (2) over the entire computational domain, using the divergence theorem, and averaging over time we find

$$A(p_{-\infty} - p_\infty) = \sum_{j=1}^{N_p} \overline{f}_j, \tag{6}$$

in which $A = (3d) \times (3d)$ is the cross-stream area of the computational domain, $N_p = 9$ the number of particles, and f_j is the component of the instantaneous hydrodynamic force on the jth particle in the mean flow direction. If $\langle \overline{f} \rangle$ is the mean force per particle, this relation gives

$$(p_{-\infty} - p_\infty) d^2 = \langle \overline{f} \rangle, \tag{7}$$

where d^2 is the area of the cross-stream section associated with each particle.

A similar procedure applied to the energy equation (3) gives

$$\rho c_p A(\overline{Tu_x}|_\infty - UT_i) = -\sum_{j=1}^{N_p} \overline{Q}_j, \tag{8}$$

where $\overline{Tu_x}|_\infty$ denotes the average value of Tu_x far downstream of the particle plane. In terms of the average heat transferred by each particle, this is

$$\rho c_p d^2(\overline{Tu_x} - UT_i) = -\langle \overline{Q} \rangle. \tag{9}$$

If the downstream boundary is taken far enough, we may expect that $\overline{Tu_x} \simeq UT_\infty$. With this approximation and (5) this relation gives

$$\frac{T_i - T_\infty}{T_i - T_p} \simeq \frac{4\pi a^2}{d^2} \frac{\mathrm{Nu}}{\mathrm{Pr}\,\mathrm{Re}_p}, \tag{10}$$

in which Nu is interpreted as the Nusselt number averaged over time and all the particles. With the present result $\mathrm{Nu} \simeq 9.72$ (see Sec. V) the fraction in the right-hand side is approximately equal to 0.0407.

IV. SIMPLIFIED POINT-PARTICLE MODEL

Before presenting the results of the simulation, it is useful to briefly discuss the predictions of a simple point-particle model, which is helpful to interpret some features of the numerical results.

We consider an infinite planar regular square array of point particles, each one separated by a distance d from its closest neighbors, located at $z = 0$, perpendicular to an incident laminar flow with constant velocity U. In view of symmetry, it is sufficient to study the problem in a domain $(-\frac{1}{2}d < x,\ y < \frac{1}{2}d,\ -\infty < z < \infty)$ with a single particle located at $x = y = z = 0$. We solve the problem in the low-Reynolds-number limit by considering the continuity equation (1) and the momentum equation in the Oseen form:

$$U\frac{\partial \hat{\mathbf{u}}}{\partial z} = -\frac{1}{\rho}\nabla p + \nu\nabla^2\hat{\mathbf{u}} - \frac{f}{\rho}\mathbf{k}\delta(x)\delta(y)\delta(z), \tag{11}$$

where $\mathbf{k}$ is a unit vector in the flow direction, f is the force exerted by the fluid on the particle, and $\hat{\mathbf{u}}$ is the perturbation velocity defined so that the three components of the velocity field in the x, y, and z directions are given by $\mathbf{u} = (\hat{u}_x, \hat{u}_y, U + \hat{u}_z)$, respectively. We consider a similar approximation

to the energy equation (3),

$$U\frac{\partial T}{\partial z} = D\nabla^2 T - \frac{Q}{\rho c_p}\delta(x)\delta(y)\delta(z), \tag{12}$$

with Q the heat absorbed by each particle from the fluid per unit time.

The solution of the problem can be expressed in the form [38–40]

$$\hat{\mathbf{u}} = -\frac{\nabla\phi}{U} + \chi\mathbf{k} - \frac{\nu}{U}\nabla\chi, \tag{13}$$

in which the scalar potential ϕ satisfies the Poisson equation

$$\nabla^2\phi = -\frac{f}{\rho}\delta(x)\delta(y)\delta(z), \tag{14}$$

and the auxiliary function χ satisfies

$$U\frac{\partial\chi}{\partial z} = \nu\nabla^2\chi - \frac{f}{\rho}\delta(x)\delta(y)\delta(z). \tag{15}$$

A remarkable aspect of this setup is the identity in form of the energy equation (12) and the equation for χ.

The solution of the problem is straightforward and is given in detail in Ref. [40]. Here it is sufficient to show the results for $\hat{u}_{L,z} = (\partial\phi/\partial z)/U$ and χ in the region downstream of the particles, $z > 0$. It is found that

$$\hat{u}_{L,z} = \frac{f}{2\rho U d^2}\left\{1 + \sum_{n=-\infty}^{\infty}\sum_{k=-\infty}^{\infty}\exp[-\lambda_{nk}z/d + 2\pi i(nx+ky)/d]\right\}, \tag{16}$$

where

$$\lambda_{nk} = 2\pi\sqrt{n^2+k^2} \tag{17}$$

and

$$\chi = -\frac{f}{\rho U d^2}\sum_{n=-\infty}^{\infty}\sum_{k=-\infty}^{\infty}\frac{\exp[-\mu_{nk}z/d + 2\pi i(nx+ky)/d]}{\sqrt{1+\frac{4\pi^2(n^2+k^2)}{(Ud/2\nu)^2}}} \tag{18}$$

with

$$\mu_{nk} = \left[\sqrt{1+\frac{4\pi^2(n^2+k^2)}{(Ud/2\nu)^2}} - 1\right]\frac{Ud}{2\nu}. \tag{19}$$

The expressions for $\hat{u}_{L,z}$ and χ show that decreasing d increases the spatial decay rate of velocity, pressure, and temperature perturbations. It is easily shown that $\mu_{nk} < \lambda_{nk}$ for any non-negative value of $Ud/2\nu$ so that the effects of pressure decay faster than those of vorticity diffusion. The character of the velocity perturbation will then be mostly determined by that of the auxiliary function χ and so will be that of the temperature perturbation in view of the similarity of the χ and temperature equations (12) and (15), respectively. In view of this similarity, one would then expect a marked parallel between the velocity perturbation and the temperature field. As will be shown below, this expectation is not borne out by the numerical results due to the finite size of the particles.

V. RESULTS

Figure 1 gives an impression of the instantaneous normalized temperature

$$T_* = \frac{T - T_p}{T_i - T_p} \tag{20}$$

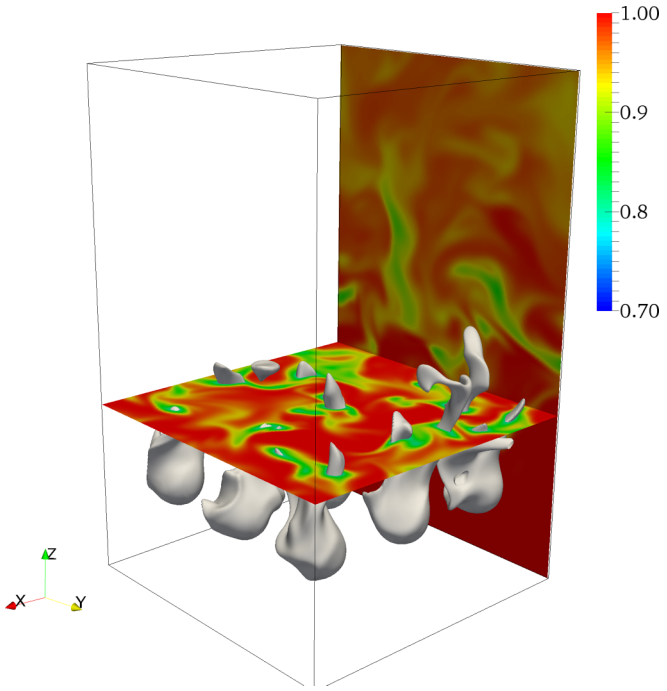

FIG. 1. Snapshot of the normalized temperature $T_* = (T - T_p)/(T_i - T_p)$ in the flow studied in this paper; the isosurfaces correspond to $T_* = 0.8$.

as found in the present simulations; the isosurfaces correspond to $T_* = 0.8$. The large regions of T_* close to 1 show that the effect of the cooling due to the particles remains mostly localized in their wakes except for the turbulent fluctuations.

The normalized time-mean temperature distribution on a plane through the centers of three contiguous particles is shown by the left diagram of Fig. 2. The right diagram permits a comparison

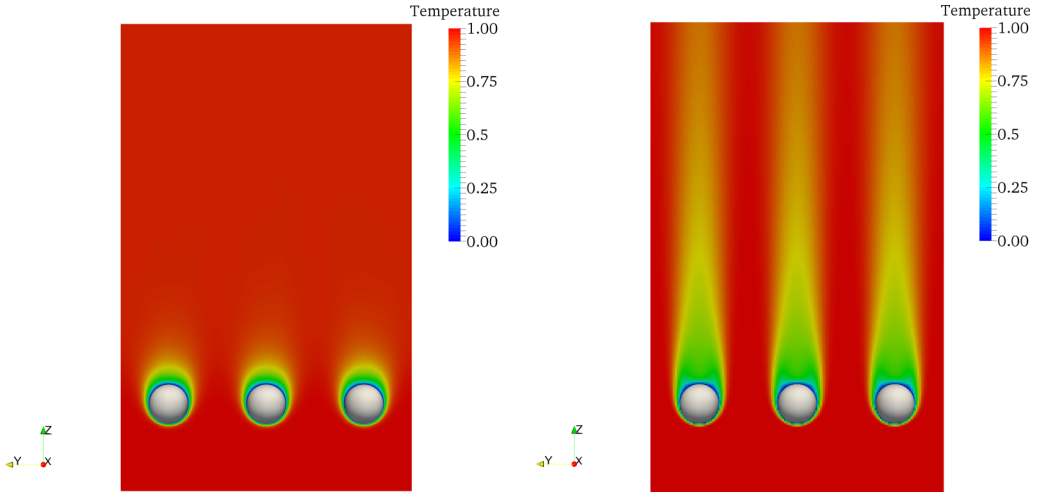

FIG. 2. Comparison between the time-mean normalized temperature distribution on a plane parallel to the mean velocity through the centers of three contiguous particles for turbulent flow (left) and for laminar flow.

TABLE II. Nusselt number predicted by several correlations for steady laminar flow past an isolated sphere and by Gunn's correlation for a sphere in a particle bed, compared with the result of the present simulations; α is the fluid volume fraction.

Correlation	Reference	Nu
$\mathrm{Nu} = 2 + 0.6\mathrm{Re}_p^{1/2}\mathrm{Pr}^{1/3}$	[41]	8.57
$\mathrm{Nu} = 2 + \left[0.4\mathrm{Re}_p^{1/2} + 0.06\mathrm{Re}_p^{2/3}\right]\mathrm{Pr}^{0.4}$	[42]	7.84
$\mathrm{Nu} = 0.922 + \left[1 + 0.1\mathrm{Re}_p^{1/3}\right]\mathrm{Re}_p^{1/3}\mathrm{Pr}^{1/3}$	[43]	8.29
Eq. (21), $\alpha = 0.97$	[44]	9.41
Eq. (21), $\alpha = 0.87$	[44]	10.1
Present result	–	9.72 ± 0.78

with the temperature distribution in the analogous steady laminar flow at the same Re_p. The great effectiveness of turbulent transport in mixing the fluid in the thermal wakes of the particle is evident here.

Table II compares the present results for the sphere Nusselt number, averaged over time and particles, with those predicted by several correlations originally developed for isolated spheres in steady laminar flow. Heat transfer is expected to be favored by turbulence, and, indeed, our results lie above those of the single-sphere laminar correlations. As noted in Ref. [11] for the case of a single sphere, the laminar-turbulent difference is not large in spite of the strong intensity of the turbulence. The small magnitude of the effect is particularly striking in view of the large differences between the laminar and turbulent thermal wakes shown in Fig. 2. It is evident that most of the heat transfer takes place on the forward portion of the sphere surface, which is affected by turbulence much less than the wake. A factor contributing to the increased heat transfer is the presence of the other spheres. Reference [44] gives a correlation for the mean single-particle Nusselt number for particles in a particle bed

$$\mathrm{Nu} = (7 - 10\alpha + 5\alpha^2)\left(1 + 0.7\mathrm{Re}_s^{0.2}\mathrm{Pr}^{1/3}\right) + (1.33 - 2.4\alpha + 1.2\alpha^2)\mathrm{Re}_s^{0.7}\mathrm{Pr}^{1/3}, \tag{21}$$

in which α is the fluid volume fraction and $\mathrm{Re}_s = \alpha\mathrm{Re}_p$ is the Reynolds number based on the superficial velocity. A straightforward application of this expression to our situation is hampered by the fact that in our case particles are not uniformly distributed in the computational domain. An effective particle volume fraction may be expected to lie between the ratio of the particle volume to the volume of a cubic box with a side equal to the interparticle spacing, which gives $\alpha \simeq 0.97$, and the ratio of the cross sectional area occupied by the particles to the cross sectional area of the domain, which gives $\alpha \simeq 0.87$. As shown in Table II, the predictions of Gunn's correlation for these two estimates of α bracket our numerical result. Due to the intensity of the turbulence, about 45%, the calculated instantaneous Nusselt number fluctuates considerably as shown in the examples of Fig. 3.

The local Nusselt number over the particle surface, defined by

$$\mathrm{Nu}_{\mathrm{loc}} = \frac{2a}{T_i - T_p}\mathbf{n}_p \cdot \nabla T, \tag{22}$$

with $\mathbf{n}_p$ the outward unit normal, averaged over time and particles, is shown in Fig. 4, where the dashed line is the result for a sphere in laminar flow at the same Re_p. Turbulence is seen to increase $\mathrm{Nu}_{\mathrm{loc}}$ at every position over the sphere surface. Just as the overall Nusselt number, this quantity also fluctuates considerably, as can be seen from the examples in Fig. 5. There are also minor variations (not shown) depending on the specific meridian along which $\mathrm{Nu}_{\mathrm{loc}}$ is calculated for each sphere.

A contour plot of the temperature field near the spheres averaged over time and over particles on planes parallel to the mean flow through the particles center is shown in Fig. 6. One notices a weak cooling of the fluid upstream of the particles and a rather short mean thermal wake. Although the

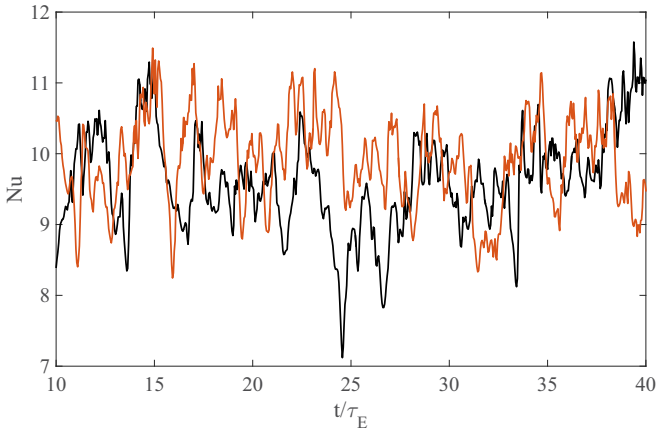

FIG. 3. Examples of the instantaneous Nusselt number vs time for two different spheres; τ_E is the eddy turnover time.

simulations of turbulent flow past an isolated sphere reported in Ref. [11] do not include results for our Reynolds number, the results for $\mathrm{Re}_p = 65$ and 250 suggest that the thermal wake in our case is indeed shorter than for an isolated sphere. The simple analytical model of the previous section, which implies that decreasing the separation between the particles shortens the thermal wake, offers a plausible explanation. The root of this behavior lies in the effect of cross-stream heat transport: the presence of the other particles limits the widening of the wake so that transport is more effective in bringing the temperature in the wake closer to that of the incident flow.

A similar contour plot for the average streamwise velocity component is shown in Fig. 7. The appearance of this figure is quite different from that for the temperature contour plot in the previous figure, which is at variance with the simple Oseen model of Sec. IV. Indeed, as noted before, this model suggests that the influence of the pressure field should decay faster than that of viscous diffusion so that the velocity distribution should be dominated by the latter. For our case of $\mathrm{Pr} = 1$ one would then expect similar results for velocity and temperature. The reason for the large difference between these two quantities is the blockage of the flow due to the finite size of the particles, an

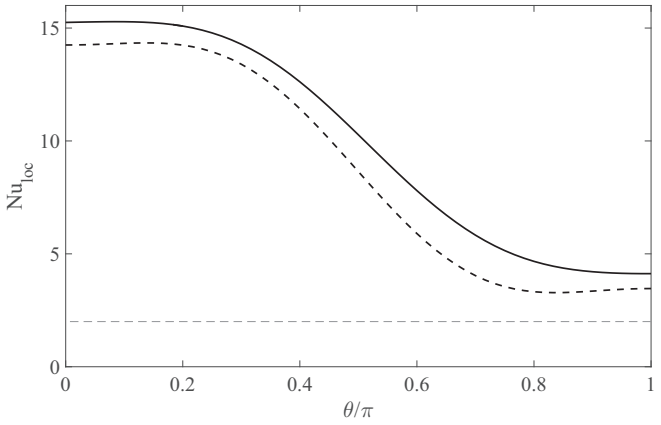

FIG. 4. Average local Nusselt number over the spheres' surface; $\theta = 0$ and π are the front and rear stagnation points, respectively. The thick dashed line is for laminar flow; the lightly dashed line is the pure conduction limit $\mathrm{Nu} = 2$.

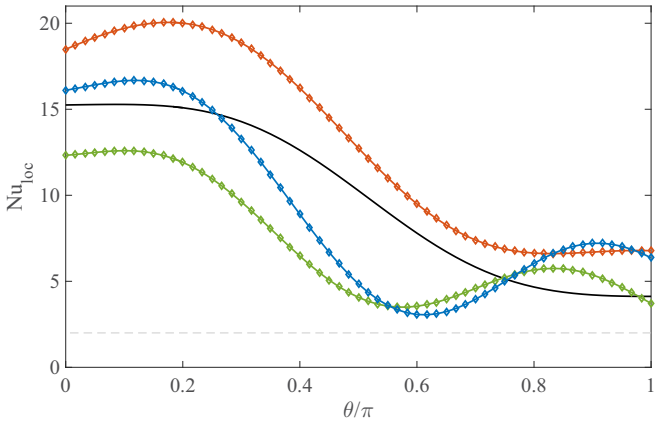

FIG. 5. Three examples of the instantaneous local Nusselt number. The solid line is the mean value shown in Fig. 4, and the lightly dashed line the pure conduction limit Nu = 2.

effect not accounted for in the Oseen model. The flow velocity increases considerably in the gap between adjacent spheres, with the consequence that the momentum wake extends considerably farther downstream than the thermal wake.

The upper diagram in Fig. 8 shows the decay of the temperature deficit $(T_i - T)/(T_i - T_p)$, averaged over time and over particles, along lines parallel to the flow direction through the particles center; the dashed line is for laminar flow. This result is very similar to that shown in Fig. 14 of Ref. [11] and matches qualitatively the exponential decrease of the temperature in a bed of fixed particles reported in Refs. [28] and [29]. Interestingly, an exponential decay is also predicted by the point-particle model of Sec. IV, where it is clearly the result of cross-stream conduction. Thus, at a crude qualitative level, one may interpret the turbulent exponential decay as the consequence of an increased turbulent diffusivity. The mean asymptotic value to which the temperature perturbation decays is found to be 0.0413, gratifyingly close to the estimate 0.0407 given earlier in (10). The solid line in the lower diagram compares the analogous quantity for the streamwise velocity, $(U - u_z)/U$, with the laminar result shown by the dashed line. The small local maxima near the particle are due to recirculation in the near-wake. For the turbulent case this line crosses the level $(U - u_z)/U = 1$ around $z/a \simeq 1.5$, which gives an estimate if the extent of the recirculation region behind the sphere. The recirculation region for the laminar case extends farther, to about $z/a = 3$. The effectiveness of the turbulent mixing process is again apparent from these results.

The probability density function (PDF) of the temperature along a line through the spheres centers parallel to mean flow is shown in Fig. 9 at different distances downstream of the spheres. Since in the present simulation the spheres are cold, the temperature at the peak of the PDF's increases with

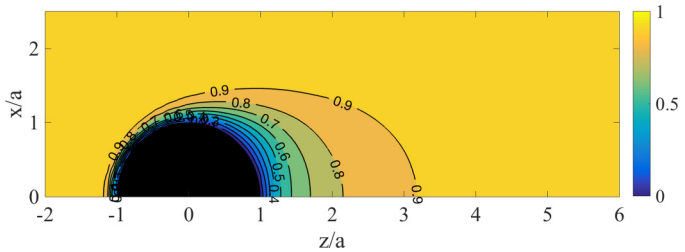

FIG. 6. Contour plot of the normalized average temperature field $(T - T_p)/(T_i - T_p)$ on a plane parallel to the flow direction through the particle center.

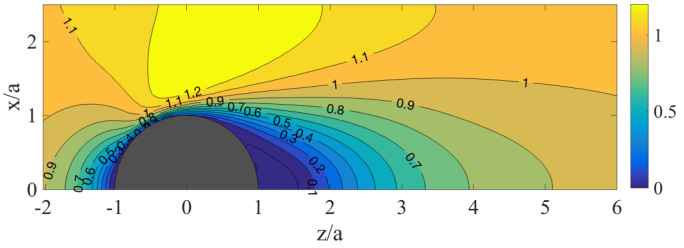

FIG. 7. Contour plot of the normalized average streamwise velocity field u_z/U on a plane parallel to the flow direction through the particle center.

downstream distance. At intermediate distances the PDF broadens, reflecting the larger velocity fluctuations unimpeded by the effect of the no-slip condition, but after a few diameters the PDF becomes very narrow and centered about the mean fluid temperature estimated earlier in (10). The recirculating flow behind the particle, which ends at about $z/a = 1.5$, does not seem to have much of an effect on these PDFs.

The analogous PDF for the normalized streamwise velocity u_z/U (Fig. 10) shows an opposite trend. Very near the sphere the velocity is slightly negative and narrowly distributed close to zero,

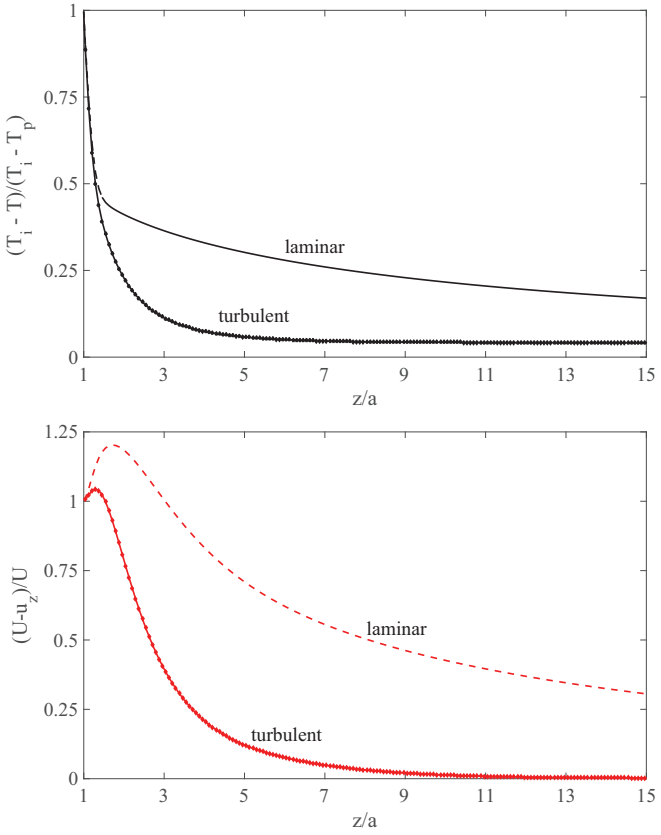

FIG. 8. Average normalized temperature deficit $(T_i - T)/(T_i - T_p)$ (upper diagram) and velocity deficit $(U - u_z)/U$, vs distance along a line through the particle center parallel to the mean flow; $z/a = 1$ is the rear stagnation point of the particle.

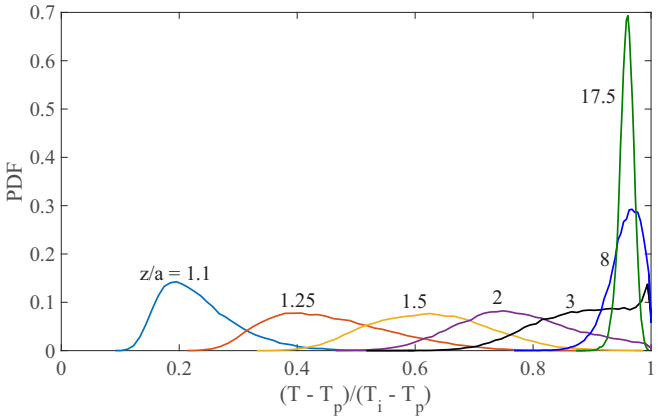

FIG. 9. Probability density function of the temperature along a line through the sphere center parallel to mean flow; the sphere center is at $z = 0$. From left to right the curves are for $z/a = 1.1$, 1.25, 1.5, 2, 3, 8, 17.5.

and it gradually recovers a mean value close to that of the incident flow downstream. Since, for the velocity, there is no effect analogous to the permanent cooling of the fluid caused by the spheres, the mean velocity far downstream must equal the mean of the incident velocity. There is a significant difference between the PDFs for z/a less than 1.5, which are in the recirculating region of the wake, and those for $z/a > 1.5$, which are much broader.

Contour plots of the root-mean-square (RMS) temperature fluctuations are shown in Fig. 11. The quantity plotted here is normalized and defined by

$$RMS(T_*) = \sqrt{\overline{(T_* - \overline{T}_*)^2}}, \tag{23}$$

with $T_* = (T - T_p)/(T_i - T_p)$. Very near the sphere, velocity and velocity fluctuations are small, and therefore so are the temperature fluctuations. Far downstream the cooling effect of the sphere is small, and therefore, again, so are the temperature fluctuations. The fluctuations are most intense in the high-velocity region close to the sphere downstream of the separation point. A small region of

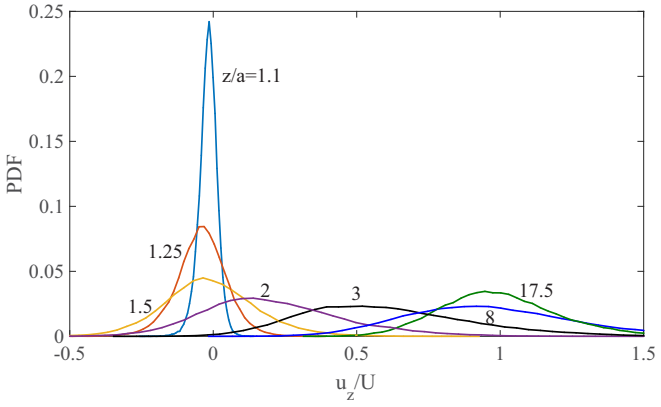

FIG. 10. Probability density function of the streamwise velocity along a line through the sphere center parallel to mean flow; the sphere center is at $z = 0$. From left to right the curves are for $z/a = 1.1$, 1.25, 1.5, 2, 3, 8, 17.5.

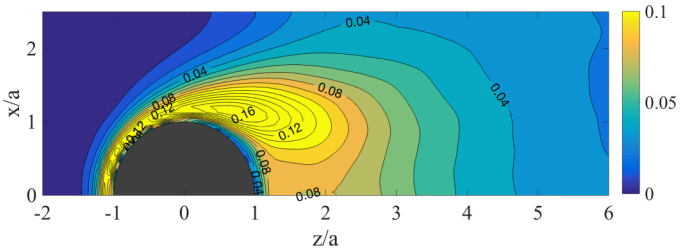

FIG. 11. Contour plots of the RMS normalized temperature fluctuations defined in (23).

relatively high fluctuations (not shown) is also found just upstream of the sphere where the region around the stagnation point is subject to the impingement of incoming eddies.

More detailed information on the decay of the RMS temperature fluctuations, defined as in (23), and normalized velocity components, $RMS(u'_{x,y,z})/U$, in the particles wake is shown in Fig. 12. The recirculating flow in the near wake contributes a small region of enhanced temperature fluctuations near the particle, evidenced by the small peak between $z/a = 1$ and 2. The two thin lines in the

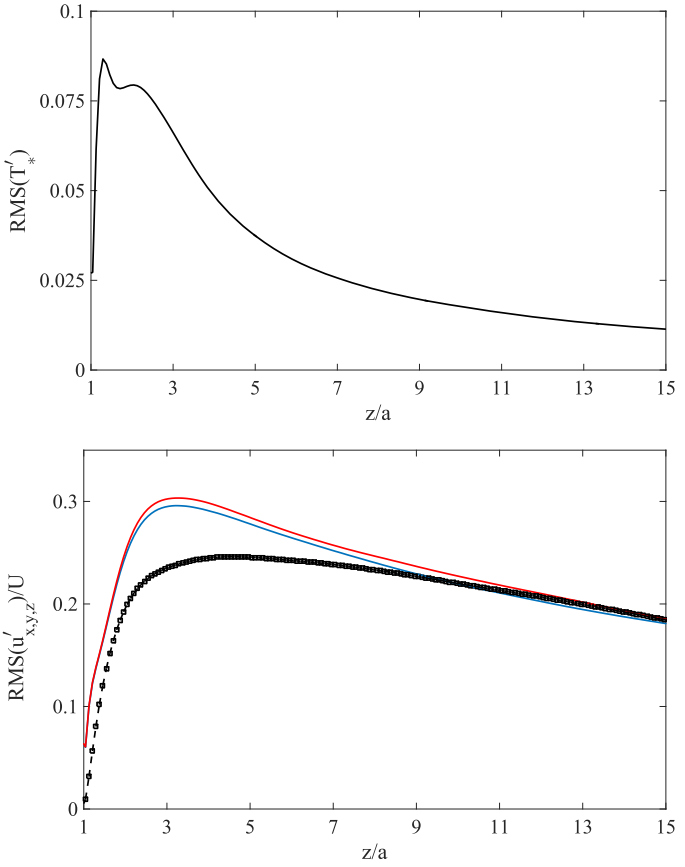

FIG. 12. Dependence of the RMS temperature (upper diagram) and velocity fluctuations vs distance along a line through the particle center parallel to the mean flow; $z/a = 1$ is the rear stagnation point of the particle. In the lower diagram the upper two lines show the fluctuations of the two cross-stream velocity components; the thick line is for the streamwise velocity.

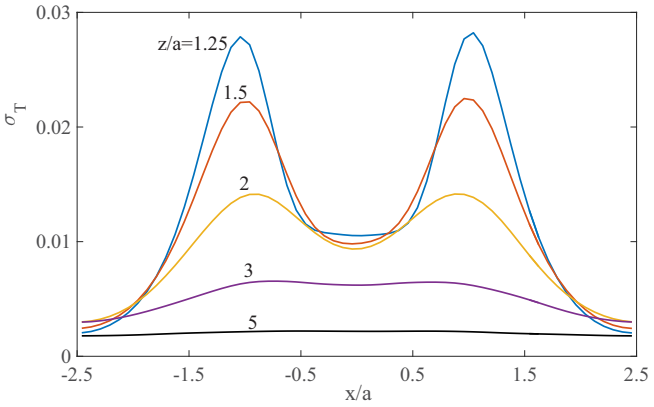

FIG. 13. Normalized temperature variance $\sigma_T = \overline{T'^2}/(T_i - T_p)^2$ in the cross-stream direction at different downstream distances from the sphere. In descending order of the maxima, the lines are for $z/a = 1.25$, 1.5, 2, 3, and 5; the particle center is on the plane $x = 0$.

lower diagram show the RMS fluctuations of the velocity components in the cross-stream directions, u'_x/U and u'_y/U. Their near identity gives an idea of the degree of convergence of the averaging used to present our results. The thick line shows the RMS of the streamwise component u'_z/U. The three results converge a few diameters downstream of the sphere, but significant differences are visible further upstream close to the recirculating region of the wake strongly buffeted by the incident turbulence.

A quantity related to fluctuations is the temperature variance $\sigma_T = \overline{T'^2}/(T_i - T_p)^2$. The distribution of this quantity in the cross-stream direction downstream of the particles is shown in Fig. 13. The maxima are located in the intensely fluctuating region already shown in Fig. 9. The decay of these features with distance is, however, very rapid as could be expected, for example, already on the basis of the left diagram of Fig. 2.

The analogous quantities for the velocity are the normalized diagonal components $u'_x u'_x/U^2$ and $u'_z u'_z/U^2$ of the Reynolds stresses. These quantities, averaged over time and particles, are shown in Fig. 14 at different distances downstream of the spheres. Both components are symmetric about the line through the particle center. The cross-stream component $u'_x u'_x/U^2$ is monotonic on both sides of the symmetry line and shows the expected broadening and shallowing of the wake with distance. The component along the mean flow, $u'_z u'_z/U^2$, on the other hand, exhibits characteristic maxima near the edges of the wake as reported in earlier studies (e.g., Ref. [36]). These structures are located outside the recirculating region of the wake but in the same range of z/a. This feature is likely rooted in the stretching and tilting of the streamlines imposed by the geometry of the sphere.

The normalized turbulent heat transport in the cross-stream directions, $\overline{u'_{x,y}T'}/U(T_i - T_p)$, is shown as a function of distance x from the sphere axis at different downstream distances in Fig. 15. The symmetry about the midplane $x = 0$ again testifies to the good convergence of the averaging. Comparison with Figs. 9, 13, and 14 shows that the maxima and minima are mostly due to the temperature rather than the velocity, fluctuations. In the case of the z component, $\overline{u'_z T'}/U(T_i - T_p)$, shown in Fig. 16, the u'_z velocity fluctuations combine with the temperature fluctuations to give somewhat stronger maxima.

The temperature variance $\overline{T'^2}$ satisfies the equation [45]

$$\frac{d\frac{1}{2}\overline{T'^2}}{dt} = -\nabla \cdot \Phi_T + \mathcal{P}_T - \epsilon_T, \tag{24}$$

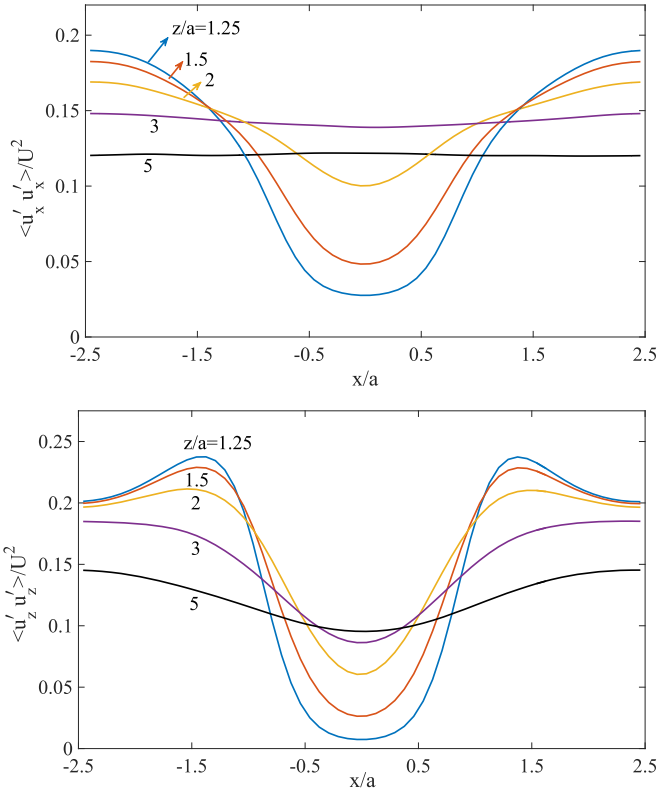

FIG. 14. Normalized diagonal turbulent Reynolds stress $u'_x u'_x/U^2$ (upper diagram) and $u'_z u'_z/U^2$ in the cross-stream planes at downstream distances from the sphere $z/a = 1.25$, 1.5, 2, 3, and 5; the particle center is on the plane $x = 0$.

in which the left-hand side is the convective derivative of the variance,

$$\Phi_T = \overline{\tfrac{1}{2}T'^2\mathbf{u}'} - \tfrac{1}{2}D\nabla\overline{T'^2} \tag{25}$$

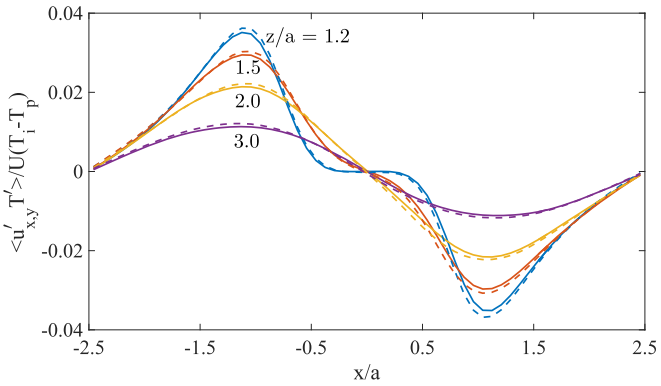

FIG. 15. Dependence of the average x (solid lines) and y components of the turbulent heat flux on distance from the sphere axis at downstream locations $z/a = 1.2$, 1.5, 2, and 3; the particle center is on the plane $x = 0$.

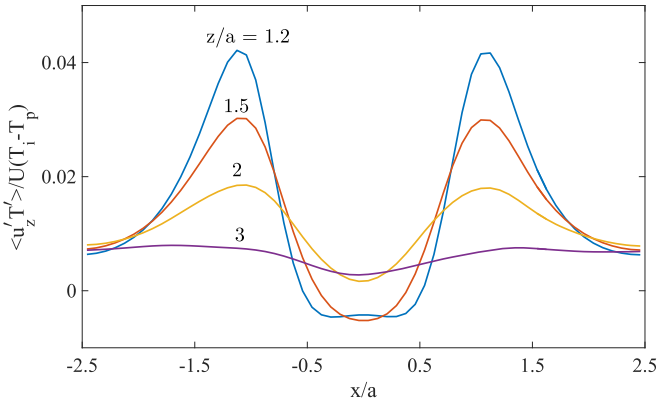

FIG. 16. Dependence of the average z-components of the turbulent heat flux on distance from the sphere axis at downstream locations $z/a = 1.2$, 1.5, 2, and 3; the particle center is on the plane $x = 0$.

is the turbulent transport,

$$\mathcal{P}_T = -\overline{T'\mathbf{u}'} \cdot \boldsymbol{\nabla}\overline{T} \tag{26}$$

is the production, and

$$\epsilon_T = D\overline{\boldsymbol{\nabla}T' \cdot \boldsymbol{\nabla}T'} \tag{27}$$

is the dissipation. Cross-stream graphs of these three terms are shown in the two panels of Fig. 17 at $z/a = 1.2$ and 1.5. The production (red line) has two relatively intense regions, one in the recirculating part of the wake and one just outside it, separated by a minimum located close to the streamline enclosing the mean recirculation. Across this line the turbulent transport (black line) changes sign.

A final point of interest concerns the time scales for mechanical and thermal energy dissipation defined by

$$\tau_m = \frac{k}{\epsilon_u}, \quad \tau_T = \frac{\frac{1}{2}\overline{T'^2}}{D\overline{\boldsymbol{\nabla}T' \cdot \boldsymbol{\nabla}T'}} = \frac{\frac{1}{2}\overline{T'^2}}{\epsilon_T}. \tag{28}$$

These two quantities, averaged over cross-stream planes, are shown as functions of the downstream distance in Fig. 18. The upper pair of lines shows τ_m with (solid) and without particles. The particles increase the energy dissipation ϵ_u and, therefore, somewhat decrease τ_m. The lowest line is the thermal timescale, which is seen to be significantly shorter than the mechanical timescale. The reason is that temperature fluctuations are confined to the particle wakes, which occupy only a relatively small fraction of the cross-stream planes, as graphically demonstrated by Fig. 1.

VI. SUMMARY AND CONCLUSIONS

We have presented the results of the resolved simulations of turbulent flow and heat transfer past a regular array of nine spheres arranged in a plane perpendicular to the mean flow. The simulations reveal a wealth of information about the character of the flow and the effectiveness of turbulence in disrupting the wakes of the spheres. This effect is graphically demonstrated in Fig. 2, which compares the thermal wakes of the spheres with and without turbulence. The upper panel of Fig. 8 conveys the same message for the temperature field, and the lower panel shows that a similar process affects the velocity field. Both the thermal and the momentum wakes are violently disrupted and shortened by the turbulent nature of the incident flow.

As reported earlier [11], the mean and local particle Nusselt numbers are found to be only moderately increased with respect to the laminar case in spite of the very intense turbulence. The

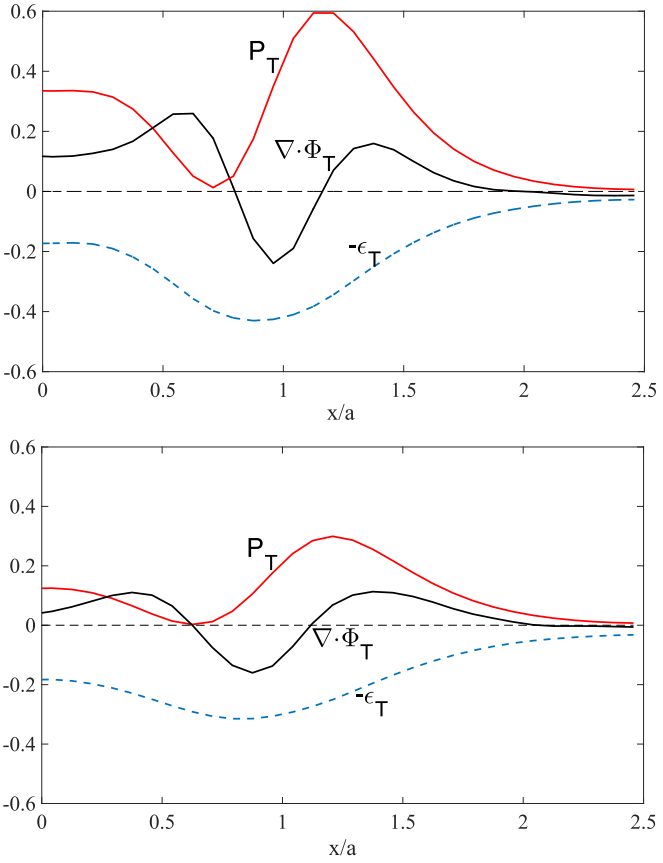

FIG. 17. The three terms in the energy budget equation (24) as functions of the cross-stream coordinate at $z/a = 1.2$ (upper diagram) and 1.5.

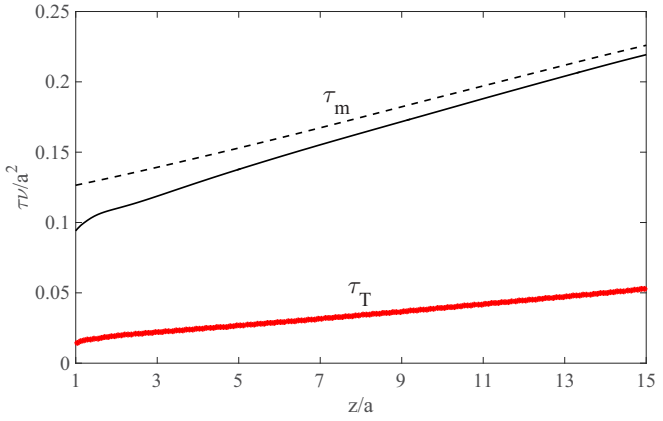

FIG. 18. Mechanical (upper two lines) and thermal time scales, defined in (28), as functions of the downstream distance; the dashed line is for turbulent flow without the particles.

temperature fluctuations are strongest near the spheres downstream of the separation line (Fig. 7). In this region the no-slip condition does not dampen the flow appreciably, and the streamline geometry imposed by the spheres' boundary stretches and tilts the incident turbulence, thereby intensifying it. As a consequence, the turbulent heat flux is particularly intense, although it is rapidly damped by the turbulence-induced mixing in the wake (Figs. 15 and 16). The enhancement of the turbulent heat flux is particularly strong in the flow direction (Fig. 16). As expected, the production term in the equation for the variance of the temperature fluctuations is largest in the regions of high temperature fluctuations and turbulent heat flux.

We have found a striking difference between the behavior of the temperature and streamwise velocity in spite of the fact that the Prandtl number considered is unity. This effect is due to the blockage of the flow caused by the spheres which has a strong effect on the velocity field but does not have a counterpart for the temperature field. The fact that, in the simple analysis of Sec. IV in which the particles are treated as points in a uniform Oseen flow, velocity and temperature are indeed similar supports this explanation. For this reason, many of the considerations developed for the behavior of passive scalars in turbulence may not be applicable to flows of this type.

The particle arrangement studied here exhibits geometric periodicity in the plane perpendicular to the incident flow. Due to the computational burden, we were able to carry out simulations only for a single nearest-neighbor center-to-center distance equal to five particle radii. Some insight into how this distance affects the results is provided by the point-particle analysis of Sec. IV, according to which decreasing the center-to-center distance increases the spatial decay rate of the temperature perturbations due to the increasing effectiveness of cross-stream conduction. To the extent that one may approximate the effect of turbulence by a crude eddy transport model, the same qualitative conclusion may be expected to hold. The simple model also predicts a similar faster decay of velocity and pressure perturbations, but this prediction may be unreliable as it does not account for the blockage caused by the finite size of the particles.

Gunn [44] has proposed the correlation (21) for the mean single-particle Nusselt number in a particle bed. Application of this relation is made somewhat uncertain by the lack of an unambiguous definition of the superficial velocity with the present geometry. Nevertheless, as shown in Sec. V and Table II, reasonable estimates of this quantity produce results that bracket the numerical ones. A simpler approach might rely on a single-particle correlation with a Reynolds number based on the superficial velocity. Here we find a similar ambiguity. With a superficial velocity based on the maximum area blockage, $\mathrm{Re}_p = 120/0.87 \simeq 138$ rather than $\mathrm{Re}_p = 120$, the Ranz-Marshall correlation [41], for example, gives for the Nusselt number the value 9.05, while the value based on $\mathrm{Re}_p = 120$ is 8.57. Our calculated result is 9.72 ± 0.78 in reasonable agreement when allowance is made for the modest increase due to the incident turbulence (cf. Fig. 4).

ACKNOWLEDGMENTS

Y.W. expresses her gratitude to Dr. Adam Sierakowski for his help with the use of the PHYSALIS code and, more generally, for his mentorship on the art of coding. This work was supported by the NSF under Grant No. CBET 1335965.

[1] F. Zonta, C. Marchioli, and A. Soldati, Time behavior of heat fluxes in thermally coupled turbulent dispersed particle flows, Acta Mech. **218**, 367 (2011).

[2] B. Arcen, A. Taniére, and M. Khalij, Heat transfer in a turbulent particle-laden channel flow, Int. J. Heat Mass Transf. **55**, 6519 (2012).

[3] S. Balachandar and J. K. Eaton, Turbulent dispersed multiphase flow, Annu. Rev. Fluid Mech. **42**, 111 (2010).

[4] M. A. van der Hoef, M. V. Annaland, N. G. Deen, and J. A. M. Kuipers, Numerical simulation of dense gas-solid fluidized beds: A multiscale modeling strategy, Annu. Rev. Fluid Mech. **40**, 47 (2008).
[5] H. P. Zhu, Z. Y. Zhou, R. Y. Yang, and A. B. Yu, Discrete particle simulation of particulate systems: A review of major applications and findings, Chem. Eng. Sci. **63**, 5728 (2008).
[6] S. C. R. Dennis, J. D. A. Walker, and J. D. Hudson, Heat transfer from a sphere at low Reynolds numbers, J. Fluid Mech. **60**, 273 (1973).
[7] R. Kurose, M. Anami, A. Fujita, and S. Komori, Numerical simulation of flow past a heated/cooled sphere, J. Fluid Mech. **692**, 332 (2012).
[8] D. S. Dandy and H. A. Dwyer, A sphere in shear flow at finite Reynolds number: Effect of shear on particle lift, drag, and heat transfer, J. Fluid Mech. **216**, 381 (1990).
[9] J. Kim and H. Choi, An immersed-boundary finite-volume method for simulation of heat transfer in complex geometries, KSME Int. J. **18**, 1026 (2004).
[10] S. D. Dhole, R. P. Chhabra, and V. Eswaran, A numerical study on the forced convection heat transfer from an isothermal and isoflux sphere in the steady symmetric flow regime, Int. J. Heat Mass Transf. **49**, 984 (2006).
[11] P. Bagchi and K. Kottam, Effect of freestream isotropic turbulence on heat transfer from a sphere, Phys. Fluids **20**, 073305 (2008).
[12] M. B. de Stadler, N. R. Rapaka, and S. Sarkar, Large eddy simulation of the near to intermediate wake of a heated sphere at Re $= 10,000$, Int. J. Heat Fluid Flow **49**, 2 (2014).
[13] R. Glowinski, T.-W. Pan, T. I. Hesla, D. D. Joseph, and J. Periaux, A fictitious domain approach to the direct numerical simulation of incompressible viscous flow past moving rigid bodies: Application to particulate flow, J. Comput. Phys. **169**, 363 (2001).
[14] M. Uhlmann, An immersed boundary method with direct forcing for the simulation of particulate flows, J. Comput. Phys. **209**, 448 (2005).
[15] W.-P. Breugem, A second-order accurate immersed boundary method for fully resolved simulations of particle-laden flows, J. Comput. Phys. **231**, 4469 (2012).
[16] S. Tenneti and S. Subramaniam, Particle-resolved direct numerical simulation for gas-solid flow model development, Annu. Rev. Fluid Mech. **46**, 199 (2014).
[17] F. Picano, W.-P. Breugem, and L. Brandt, Turbulent channel flow of dense suspensions of neutrally buoyant spheres, J. Fluid Mech. **764**, 463 (2015).
[18] A. J. Sierakowski and A. Prosperetti, Resolved-particle simulation by the Physalis method: Enhancements and new capabilities, J. Comput. Phys. **309**, 164 (2016).
[19] M. Uhlmann and A. Chouippe, Clustering and preferential concentration of finite-size particles in forced homogeneous-isotropic turbulence, J. Fluid Mech. **812**, 991 (2017).
[20] Z. Yu, X. Xiao, and A. Wachs, A fictitious domain method for particulate flows with heat transfer, J. Comput. Phys. **217**, 424 (2006).
[21] Z. G. Feng and E. E. Michaelides, Inclusion of heat transfer computations for particle laden flows, Phys. Fluids **20**, 040604 (2008).
[22] Z. G. Feng and E. E. Michaelides, Heat transfer in particulate flows with direct numerical simulation (DNS), Int. J. Heat Mass Transf. **52**, 777 (2009).
[23] Z. Wang, J. Fan, K. Luo, and K. Cen, Immersed boundary method for the simulation of flows with heat transfer, Int. J. Heat Mass Transf. **52**, 4510 (2009).
[24] N. G. Deen, S. H. L. Kriebitzsch, M. A. van der Hoef, and J. A. M. Kuipers, Direct numerical simulation of flow and heat transfer in dense fluid-particle systems, Chem. Eng. Sci. **81**, 329 (2012).
[25] N. G. Deen, E. A. J. F. Peters, J. T. Padding, and J. A. M. Kuipers, Review of direct numerical simulation of fluid-particle mass, momentum and heat transfer in dense gas-solid flows, Chem. Eng. Sci. **116**, 710 (2014).
[26] H. Tavassoli, S. H. L. Kriebitzsch, M. A. van der Hoef, E. A. J. F. Peters, and J. A. M. Kuipers, Direct numerical simulation of particulate flow with heat transfer, Int. J. Multiphase Flow **57**, 29 (2013).
[27] S. Tenneti, B. Sun, R. Garg, and S. Subramaniam, Role of fluid heating in dense gas-solid flow as revealed by particle-resolved direct numerical simulation, Int. J. Heat Mass Transf. **58**, 471 (2013).

[28] Z. G. Feng and S. G. Musong, Direct numerical simulation of heat and mass transfer of spheres in a fluidized bed, Powder Technol. **262**, 62 (2014).
[29] B. Sun, S. Tenneti, S. Subramaniam, and D. L. Koch, Pseudo-turbulent heat flux and average gas-phase conduction during gas-solid heat transfer: Flow past random fixed particle assemblies, J. Fluid Mech. **798**, 299 (2016).
[30] Y. Wang, A. J. Sierakowski, and A. Prosperetti, Fully-resolved simulation of particulate flows with particles-fluid heat transfer, J. Comput. Phys. **350**, 638 (2017).
[31] M. N. Ardekani, O. Abouali, F. Picano, and L. Brandt, Heat transfer in laminar Couette flow laden with rigid spherical particles, J. Fluid Mech. **834**, 308 (2018).
[32] K. Gudmundsson and A. Prosperetti, Improved procedure for the computation of Lamb's coefficients in the Physalis method for particle simulation, J. Comput. Phys. **234**, 44 (2013).
[33] S. Lundgren, Linearly forced isotropic turbulence, in *Annual Research Briefs* (Stanford University, Stanford, CA, 2003), p. 461.
[34] C. Rosales and C. Meneveau, Linear forcing in numerical simulations of isotropic turbulence: Physical space implementations and convergence properties, Phys. Fluids **17**, 095106 (2005).
[35] P. L. Carroll and G. Blanquart, A proposed modification to Lundgren's physical space velociy forcing method for isotropic turbulence, Phys. Fluids **25**, 105114 (2013).
[36] L. Botto and A. Prosperetti, A fully resolved numerical simulation of turbulent flow past one or several spherical particles, Phys. Fluids **24**, 013303 (2012).
[37] Y. Wang, A. J. Sierakowski, and A. Prosperetti, Rotational dynamics of a particle in a turbulent stream (unpublished).
[38] P. A. Lagerstrom, Laminar flow theory, in *Theory of Laminar Flows*, edited by F. K. Moore (Princeton University Press, Princeton, 1964), pp. 88–102.
[39] A. Prosperetti, Laminar flow at large distances from an infinite two-dimensional grid, J. Mécanique **15**, 209 (1976).
[40] Y. Wang and A. Prosperetti, Laminar flow and heat transfer past an infinite planar array of point particles (unpublished).
[41] W. E. Ranz and W. R. Marshall, Evaporation from drops, part II, Chem. Eng. Prog. **48**, 173 (1952).
[42] S. Whitaker, Forced convection heat transfer correlations for flow in pipes, past flat plates, single cylinders, single spheres, and for flow in packed beds and tube bundles, AIChE J. **18**, 361 (1972).
[43] Z. G. Feng and E. E. Michaelides, A numerical study on the transient heat transfer from a sphere at high Reynolds at Péclet numbers, Int. J. Heat Mass Transf. **43**, 219 (2000).
[44] D. J. Gunn, Transfer of heat or mass to particles in fixed and fluidised beds, Int. J. Heat Mass Transf. **21**, 467 (1978).
[45] S. B. Pope, *Turbulent Flows* (Cambridge University Press, Cambridge, 2000).